

How simple can you go? An off-the-shelf transformer approach to molecular dynamics

Max Eissler^{1,2}, Tim Korjakow^{1,2}, Stefan Ganscha⁵, Oliver Unke⁵, Klaus-Robert Müller^{1,2,3,4,5}, and Stefan Gugler*^{1,2}

¹BIFOLD – Berlin Institute for the Foundations of Learning and Data

²Machine Learning Group, Technische Universität Berlin

³Department of Artificial Intelligence, Korea University

⁴Max-Planck Institute for Informatics

⁵Google DeepMind

Feb 25, 2025

Abstract

Most current neural networks for molecular dynamics (MD) include physical inductive biases, resulting in specialized and complex architectures. This is in contrast to most other machine learning domains, where specialist approaches are increasingly replaced by general-purpose architectures trained on vast datasets. In line with this trend, several recent studies have questioned the necessity of architectural features commonly found in MD models, such as built-in rotational equivariance or energy conservation. In this work, we contribute to the ongoing discussion by evaluating the performance of an MD model with *as few specialized architectural features as possible*. We present a recipe for MD using an Edge Transformer, an “off-the-shelf” transformer architecture that has been minimally modified for the MD domain, termed MD-ET. Our model implements neither built-in equivariance nor energy conservation. We use a simple supervised pre-training scheme on ~ 30 million molecular structures from the QCML database. Using this “off-the-shelf” approach, we show state-of-the-art results on several benchmarks after fine-tuning for a small number of steps. Additionally, we examine the effects of being only approximately equivariant and energy conserving for MD simulations, proposing a novel method for distinguishing the errors resulting from non-equivariance from other sources of inaccuracies like numerical rounding errors. While our model exhibits runaway energy increases on larger structures, we show approximately energy-conserving NVE simulations for a range of small structures.

1 Introduction

Molecular dynamics (MD) simulations are essential for understanding molecular behavior [1, 2, 3], such as molecular relaxation [4], predicting structure [5], modeling interactions [6], replicating spectra [7], up to protein folding and design [8, 9, 10]. Machine Learning (ML) models can be used as heuristic approximations of the Schrödinger equation thereby significantly accelerating accurate MD simulations (e.g. Rupp et al. [11], Noé et al. [12], Unke et al. [13], Keith et al. [14], Unke et al. [15]). To ensure physical consistency of predictions, researchers have focused on incorporating inductive biases into MD models, which restrict models to physically plausible solutions [16, 17, 18, 19, 20, 13]. For instance, rotational equivariance guarantees that if a molecule is rotated, the forces are rotated as well (e.g. Schütt et al. [21], Bronstein et al. [22], Unke et al. [23]). Meanwhile, many other ML domains are increasingly using unconstrained, general-purpose architectures and large amounts of training data [24, 25, 26].

Several recent theoretical [27, 28] and empirical works [29, 30, 31, 32] discuss the necessity of commonly used physical constraints and inductive biases in MD models, most notably $SO(3)$ -equivariance and energy conservation. For example, architectures predicting non-conservative forces include ForceNet [33], GemNet-dT [34], Orb [35] or Equiformer [36]. However, to the best of our knowledge, no architectures that fully embrace the general-purpose paradigm have been presented so far. We contribute by studying

*Corresponding author: stefan.gugler@tu-berlin.de

an extreme case: *We present and evaluate the best MD model we can build using a minimal amount of MD-specific design features.* Specifically, we aim to use an architecture that could be used in some other ML setting with minimal changes.

The “off-the-shelf” recipe we use is simple: We modify an Edge Transformer (ET) [37, 38] with MD-specific embedding layers and train on the new QCML database [39]. QCML has an unprecedented size and range across the periodic table, including out-of-equilibrium structures, different spin and charge states, and includes properties for a subset of ~ 30 million entries calculated with density functional theory accuracy at the PBE0 level [40, 41] (including dispersion corrections [42, 43]). During training, we use two randomly rotated and mirrored copies of each sampled structure, so that our model can learn approximate $O(3)$ -equivariance. Instead of predicting a combined loss [44] of energies and forces or calculating forces as the (negative) gradient of the predicted energy with respect to positions, we predict forces directly. This approach does not guarantee that the predicted forces are energy-conserving, but it improves the speed of the model, because forces need not be calculated by automatic differentiation. For downstream task evaluation, we fine-tune the model for a small number of steps only.

For MD simulations, we evaluate either the pre-trained model without further training (zero-shot) or fine-tune on a small number of samples of the target structure (few-shot). To increase the accuracy during MD simulations, we use a frame-averaging approach [45] over the $SO(3)$ group to achieve an approximate “post-hoc” equivariance and further correct the predicted forces to guarantee no spurious rigid rotational or translational motion is introduced over time.

Our contributions are as follows:

1. We present an MD-adapted Edge Transformer (MD-ET) and show that our implementation can achieve competitive performance on several common benchmarks. We also demonstrate sample-efficiently finetuning.
2. We examine the effects of forgoing almost all commonly used inductive biases. Specifically, we evaluate the effects of being only approximately equivariant and energy-conserving in detail. We present a novel evaluation framework that is able to quantify deviations from true equivariance and distinguish them from effects stemming from model inaccuracy and numerical noise.
3. We present a comparison of MD-ET with an identically pretrained equivariant and energy-conserving model, highlighting the impact of removing physical constraints on MD simulations.

2 Background

While incorporating physics-inspired inductive biases into MLFF models yields powerful and data-efficient architectures, they also impose constraints. For instance, directly predicting (non-conservative) rotationally equivariant forces restricts a model to only performing equivariant operations [46]. A more subtle downside of specialized architectures is the increased difficulty to transfer advances from other ML research and profit from improved hardware and software tools. Engineering complexity was recently cited as the reason the AlphaFold project removed its equivariant inductive biases [10, 8]. Since protein conformer prediction is thematically close to MD, this prompted the discussion of which inductive biases are essential to the MD domain: Questioning the need for equivariance, Langer et al. [47] find that data augmentation during training can achieve a high degree of approximate equivariance in molecular dynamics. Neumann et al. [35] present Orb, a completely unconstrained message-passing architecture with outstanding benchmark performance. Elhag et al. [31] show that an additional loss term to induce equivariance combined with data augmentation results in competitive performance and approximate equivariance. Several theoretical works also suggest that unconstrained models can produce equivariant outputs under certain circumstances Gerken and Kessel [27], Nordenfors and Flinth [28], Puny et al. [45]. In contrast, the performance effects of removing energy conservation are less clear. Although benchmarking results suggest non-conservative models can perform stable MD simulations [35]. Bigi et al. [29] report that all non-conservative models in their study suffer from runaway temperature increases and thus instability.

Several current debates in the MD field center around competing paradigms – one leveraging inductive biases for sample efficiency, and another prioritizing simplicity, scale and transfer using general-purpose models. Recently, several aspects of the scaling paradigm have been studied and discussed in isolation

[47, 29, 32]. Our work advances this discourse by empirically evaluating a simple baseline approach that fully adopts the scaling paradigm for MD and exploring its limits.

3 Molecular Dynamics Edge Transformer

We use the transformer, an architecture which has proven to scale well in many domains, as a starting point in our design process. We decide to use the Edge Transformer variant introduced by Bergen et al. [37] for algorithmic reasoning and adapted by Müller et al. [38] for graph learning, employing a higher-order attention mechanism instead of self-attention due to its expressivity (see below). We modify only the ET’s embeddings for MD. We therefore name our variant MD-ET.

Expressivity Expressivity describes the ability of an ML model to tell the difference between two non-equivalent inputs, i.e., to distinguish two graphs that are not isomorphic. Morris et al. [48] show that the expressivity of a graph learning model can be related to performing a variant of the Weisfeiler-Leman (WL) graph isomorphism test. Hordan et al. [49] extend the WL-test to equivariant point clouds and show that a cutoff-free model with 3-WL expressivity is universal on 3D point clouds, i.e., such a model can theoretically learn to distinguish any two 3D point clouds. Müller et al. [38] show the ET has an expressive power equivalent to 3-WL. The ET can thus universally distinguish 3D point clouds, making it theoretically well-suited as an MLFF.

Tokenization The ET derives its name from its tokenization scheme. We represent a molecular system as the set of all edges of a fully connected graph, that is, all pairs of atoms (including self-loops). We then encode the molecular system as a three-dimensional tensor $\mathbf{X} \in \mathbb{R}^{N \times N \times D}$, where N denotes the number of atoms in the system and D is the embedding dimension. An embedding S_{ij} thus represents the edge between atoms i and j , while S_{ii} represents the atom i .

Triangular Attention Mechanism To achieve the expressive power of 3-WL, the ET performs updates on the three-dimensional tensor representation described in the previous paragraph using a triangular attention mechanism, performing interactions between triples of atoms,

$$\text{TRIA}(\mathbf{x}_{ij}) = \sum_{l=1}^N \alpha_{ilj} \mathbf{V}_{ilj} . \quad (1)$$

Triangular attention is defined as a tensor product between an attention tensor $\alpha \in \mathbb{R}^{N \times N \times N}$ and a value tensor $\mathbf{V} \in \mathbb{R}^{N \times N \times D}$. An element of the attention tensor is calculated as

$$\alpha_{ilj} = \text{softmax}_{l \in [N]} \left(\frac{1}{\sqrt{d}} \mathbf{x}_{il} \mathbf{W}^Q \left(\mathbf{x}_{lj} \mathbf{W}^K \right)^\top \right) \in \mathbb{R} , \quad (2)$$

i.e., the attention score between the representations of edges (i, l) and (l, j) and where the notation $[N]$ represents the set $\{1, 2, \dots, N\}$. The value vector

$$\mathbf{v}_{ilj} = \mathbf{x}_{il} \mathbf{W}^{V_1} \odot \mathbf{x}_{lj} \mathbf{W}^{V_2} \in \mathbb{R}^D \quad (3)$$

is a combination of the value vectors of \mathbf{x}_{il} and \mathbf{x}_{lj} through elementwise multiplication. $\mathbf{W}^Q, \mathbf{W}^K, \mathbf{W}^{V_1}, \mathbf{W}^{V_2} \in \mathbb{R}^{d \times d}$ are learned weight matrices [38]. The triangular attention mechanism extends to multi-head attention analogous to regular self-attention. Similarly, a full ET layer is defined analogously to a transformer layer [50]; specifically,

$$\mathbf{x}_{ij}^{(t)} = \text{FFN} \left(\text{TRIA} \left(\text{LN} \left(\mathbf{x}_{ij}^{(t-1)} \right) \right) + \mathbf{x}_{ij}^{(t-1)} \right) , \quad (4)$$

where FFN is a feed-forward neural network and LN denotes layer norm [51].

The triangular attention is straightforward to implement and JIT-compile (see Appendix A.2). The large 3D tensor products are embarrassingly parallelizable and thus execute very efficiently on accelerators. This makes the ET comparatively fast despite a runtime and memory complexity of $\mathcal{O}(N^3)$, where N is the number of atoms in the system (see Appendix A.3).

Molecular Embeddings To generate initial edge representations, we combine several embeddings: i) spin and charge, ii) atomic numbers, iii) pairwise distances, and iv) pairwise displacement vectors. To maintain MD-ET’s simplicity we implement commonly used embedding layer where possible. For details, see Appendix A.2.1.

4 Experiments

To contribute to the current discussion about inductive biases in MD, we need to thoroughly evaluate MD-ET. Specifically, we want to address the following questions:

- **Q1:** Can an “off-the-shelf” model without inductive biases compete on common benchmarks measuring accuracy, inference speed, and MD stability?
- **Q2:** How equivariant is MD-ET? Is approximate equivariance likely to impact MD simulation stability?
- **Q3:** Is MD-ET approximately energy-conserving? How affected is the stability of MD simulations?
- **Q4:** How faithful are MD simulations? Is there a correlation between energy conservation and observables?

4.1 Pretraining

We use a pretrained model for all downstream evaluations. However, instead of the commonly used denoising task [52, 35] we perform supervised pretraining on the new QCML dataset [39]. We create an approximate 90%/5%/5% split from QCML. As QCML contains multiple conformations for each structure sampled along their normal modes, we ensure that all conformations of a structure get assigned to the same split.

To learn approximate equivariance, we use data augmentation: During pretraining we duplicate each batch once and apply random rotations and reflections to both copies to form an augmented batch. We train MD-ET for 880k steps on QCML using a batch size of 1024 (i.e., 512 before data augmentation), which takes approximately 16 A100 GPU-days (see Appendix A.5).

4.2 Postprocessing

Our model does not require any modifications for downstream fine-tuning tasks. For MD-simulations we apply two techniques to enhance model predictions:

Net Force and Torque Removal We adopt the net force and torque removal algorithm described in [35]. We find that removing net forces and torque from model predictions improves the stability of MD simulations, while only increasing the time of a model evaluation by 10-20 percent (see Appendix A.3). We use net force and torque removal in all simulation experiments.

Frame-averaging For some simulations, we observe that frame-averaging [45] helps to improve MD stability. For frame-averaging we use M rotation matrices to pass M different orientations of the input positions to the model. We then apply the inverse rotations to the predicted forces and average them. We discuss the effects of frame-averaging in section 4.4. We use frame-averaging only where explicitly stated. For implementation details, see section 4.4 and Appendix A.5.

4.3 Q1: Benchmark Results

We evaluate the performance of our proposed MD-ET model across several standard molecular dynamics benchmarks. We compare MD-ET with established MLFFs, focusing on their accuracy, stability and efficiency. Our experiments cover a range of datasets, including QCML [39], MD17 [16], and Ko2020 [53], each presenting distinct challenges.

Performance on the QCML Dataset

In Table 1, we present the mean absolute error (MAE) of force predictions for MD-ET, SpookyNet [13], and PaiNN [21].

Table 1: Force prediction test MAE on the QCML dataset in kcal/mol \AA^{-1} for different models.

Model	Test MAE
MD-ET	0.69
SpookyNet [†]	0.74
PaiNN	0.98

[†]Does not separate conformers between training and testing.

Table 2: Performance comparison on the MD17 benchmark on stability (ps) with a maximum at 300 ps, force MAE (meV \AA^{-1}) and FPS. Higher is better is denoted (\uparrow) and vice versa. Best average results in bold. Results marked with a * indicate that the molecule was included in the pretrain train split.

Metric	Molecule	DeepPot-SE [54]	SchNet [17]	DimeNet [55]	PaiNN [21]	SphereNet [56]	ForceNet [33]	GemNet-dT [34]	NequIP [57]	MD-ET (pretrained) (ours)	MD-ET (finetuned) (ours)
Stability (\uparrow)	Aspirin	9	26	54	159	141	182	192	300	154	300
	Ethanol	300	247	26	86	33	300	300	300	300	300
	Naphthalene	246	18	85	300	6	300	25	300	256	300
	Salicylic Acid	300	300	73	281	36	1	94	300	213	300
	Average	213.8	147.8	60.0	206.5	54	195.8	152.8	300	230.8	300
MAE (\downarrow)	Aspirin	21.0	35.6	10.0	9.2	3.4	22.1	5.1	2.3	4.2	4.2
	Ethanol	8.9	16.8	4.2	5.0	1.7	14.9	1.7	1.3	2.5	1.0*
	Naphthalene	13.4	22.5	5.7	3.8	1.5	9.9	1.9	1.1	4.0	2.3
	Salicylic Acid	14.9	26.3	9.6	6.5	2.6	12.8	4.0	1.6	3.3	2.8
	Average	14.6	25.3	7.4	6.1	2.3	15.0	3.2	1.6	3.5	2.6
FPS (\uparrow)	Aspirin	88.0	108.9	20.6	85.8	17.5	137.3	56.8	8.4	159.8	159.8
	Ethanol	101.0	112.6	21.4	87.3	30.5	141.1	54.3	8.9	148.1	148.1
	Naphthalene	109.3	110.9	19.1	92.8	18.3	140.2	53.5	8.2	150.2	150.2
	Salicylic Acid	94.6	111.7	19.4	90.5	21.4	143.2	52.4	8.4	147.3	147.3
	Average	98.2	111.0	20.1	89.1	21.9	140.5	54.3	8.5	151.4	151.4

MD-ET achieves the lowest MAE among the compared models, outperforming both SpookyNet and PaiNN. We observe that SpookyNet’s results do not separate conformers between training and testing, which may overestimate generalization performance. This improvement over equivariant models like PaiNN and SpookyNet suggests that approximate equivariance, as utilized in MD-ET, does not hinder performance on such benchmarks. However, a low test error does not necessarily imply a low MD simulation error or a stable trajectory, as we will demonstrate below.

MD17-10k: molecule specific results

The MD17 dataset [16] consists of molecular dynamics trajectories for small organic molecules and has been proposed as a benchmark by Fu et al. [58], challenging models to not only predict a low force error but also measures stability, i.e., how long a simulation experiences no catastrophic failure. The third criterion is speed, i.e., how many times per second the model can be evaluated. Table 2 compares MD-ET with several state-of-the-art models, including NequIP [57], GemNet-dT [34]. In addition to training ET-MD directly on MD17, we also report fine-tuning results after 2000 fine-tuning steps (see Appendix A.6 for details). Since there is some overlap with the pretraining set, fine-tuning results for ethanol (marked with a *), have only limited significance.

MD-ET achieves force MAEs similar to those of NequIP and GemNet-dT (which is also not energy-conserving). The only other model that violates energy conservation is ForceNet at a much higher MAE. While NequIP attains slightly lower MAEs, MD-ET excels in computational efficiency, processing over 150 frames per second (FPS) beating all other models. MD-ET also reaches the maximum simulation stability score across all molecules. While a 300 ps NVT simulation is not sufficient to assess the long-term stability of MD trajectories, it can still be used to compare the stability of different models.

MD17@CCSD(T)

For molecular dynamics (MD) simulations where precise electron correlation is necessary to accurately model potential energy surfaces and critical interactions, such as transition states, Density Functional Theory (DFT) reference data may not always be sufficiently accurate. The CCSD(T) level of theory

Table 3: MAE of atomic forces (meV \AA^{-1}) for MD17 molecules recalculated with CCSD(T). Best results in bold. Molecules with a * are included in the pretrain dataset of MD-ET.

Molecule	sGDML [20]	GemNet-Q [34]	GemNet-T [34]	NewtonNet [59]	NequIP [57]	MD-ET (1000 samples) (ours, finetuned)	MD-ET (100 samples) (ours, finetuned)
Ethanol*	15.0164	3.0814	3.0814	10.2424	2.9946	1.4683 \pm 0.0017	2.5756 \pm 0.0045
Aspirin	33.0274	10.4160	10.3292	15.4504	8.2894	4.9525 \pm 0.0069	9.0772 \pm 1.0465
Benzene	1.8228	0.6944	0.6944	0.4774	0.2604	2.0507 \pm 0.0645	2.7354 \pm 0.0123
Malonaldehyde	16.2316	4.3400	5.9024	12.3690	4.5136	2.5632 \pm 0.0158	5.1715 \pm 0.0688
Toluene	8.8970	2.5172	2.6908	3.4720	1.6926	2.6117 \pm 0.0072	4.3461 \pm 0.0062

Table 4: RMSEs of atomic forces (meV \AA^{-1}) for different molecular systems, comparing 4G-BPNN, SpookyNet, and our work. The values for 4G-BPNN are taken from [53]. Best results in bold.

Molecule	4G-BPNN [53]	SpookyNet [13]	MD-ET (ours, finetuned)
$\text{C}_{10}\text{H}_2/\text{C}_{10}\text{H}_3^+$	78.00	5.802	5.122 \pm 0.197
$\text{Na}_8/\text{Cl}_8^+$	32.78	1.052	2.26 \pm 0.014
$\text{Ag}_3^{+/-}$	31.69	26.64	11.78 \pm 0.409
$\text{Au}_2\text{-MgO}$	66.0	5.337	-

is often regarded as the ‘‘gold standard’’ of quantum chemistry and is thus a suitable choice for these cases. Nonetheless, the substantial computational cost of CCSD(T) renders it impractical for large-scale or long-duration simulations. Transfer learning from lower-level theories, such as DFT, presents an effective strategy to approximate CCSD(T) using the expensive CCSD(T) samples efficiently. We use the MD17@CCSD(T) dataset [20], which recalculates trajectories for molecules in MD17 using CCSD(T) to test this approach using MD-ET. Although MD-ET was pretrained on the PBE0 level, Table 3 demonstrates that MD-ET can effectively capture higher-level interactions through fine-tuning with a limited number of CCSD(T) samples. When fine-tuned on 1,000 CCSD(T)-level samples, MD-ET achieves lower mean absolute error (MAE) than all competing models for three of the five structures. For toluene, its MAE is comparable to GemNet-T, while for benzene, it exhibits the highest error among the benchmarked models. Furthermore, when we reduce the fine-tuning dataset by an order of magnitude MD-ET still reaches accuracy comparable to models trained on the full dataset.

Ko2020: molecule specific results

Ko et al. [53] introduce a molecular dataset consisting of molecular (e.g. C_{10}H_2 and C_{10}H^+) and metallic systems (e.g., $\text{Ag}_3^{+/-}$), which are typically challenging for conventional MLFFs. Table 4 compares the force root mean squared errors (RMSE) of MD-ET with 4G-BPNN [53] and SpookyNet [13] on selected systems from the Ko2020 dataset.

For the $\text{C}_{10}\text{H}_2/\text{C}_{10}\text{H}_3^+$ and $\text{Ag}_3^{+/-}$ systems, MD-ET outperforms both 4G-BPNN and SpookyNet. This demonstrates MD-ET’s capability to model smaller ionic and metallic systems. However, on the $\text{Na}_8/\text{Cl}_8^+$ MD-ET’s performance is slightly worse and fails to converge on $\text{Au}_2\text{-MgO}$ systems.

4.4 Q2: Equivariance Evaluation

Our model, MD-ET, is only approximately equivariant. Although MD-ET’s performs well on benchmarks, we examine the potential influence of approximate equivariance on MD simulations more closely. To quantify how (non-)equivariant our model is, we define the equivariance error as the expected Euclidean distance between the model’s prediction on a randomly rotated input and the expected prediction averaged over all rotations in the symmetry group,

$$E_{\text{eq}}(D, \hat{f}_\theta) = \mathbb{E}_{x \sim D} \left[\left\| \mathbb{E}_{\mathcal{R} \sim \text{SO}(3)} [\mathcal{R}^\top \hat{f}_\theta(\mathcal{R}x)] - \mathcal{S}^\top \hat{f}_\theta(\mathcal{S}x) \right\|_2 \right], \quad (5)$$

where $x \sim D$ are the 3D positions sampled from their distribution D , $\mathcal{R}, \mathcal{S} \sim \text{SO}(3)$ are rotation matrices, and \hat{f}_θ is a trained predictor. For a perfectly equivariant model, $E_{\text{eq}} = 0$ (proof in Appendix A.4).

In practice, models use floating point arithmetic with finite precision and numerical inaccuracies accumulate during evaluation. For this reason, equivariant models do not reach $E_{\text{eq}} = 0$. To better assess MD-ET’s

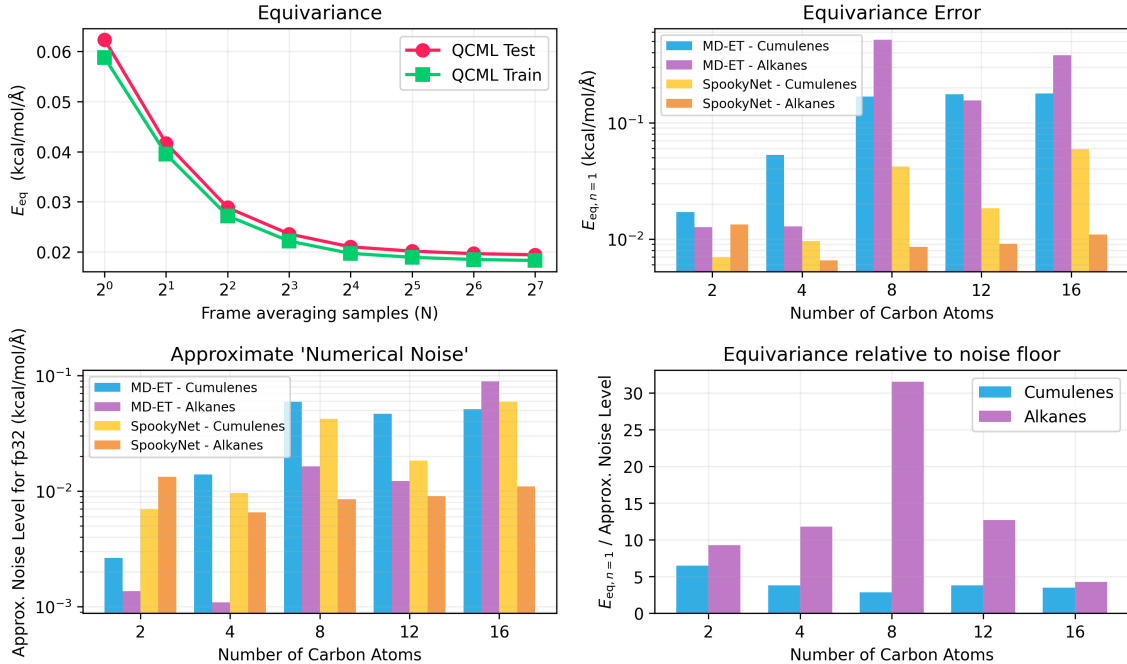


Figure 1: Equivariance Evaluation. **Top Left:** Average equivariance error E_{eq} for 2048 randomly sampled QCML train and test structures using different frame-averaging sample sizes n . **Top Right:** Equivariance error (without frame averaging) over the $\text{SO}(3)$ group across a range of alkanes and cumulenes. **Bottom Left:** Approximate numerical noise level over the $\text{SO}(3)$ group for alkanes and cumulenes. **Bottom Right:** Relative equivariance error for alkanes and cumulenes.

deviation from an equivariant architecture, we evaluate E_{eq} using different amounts of frame-averaging (see section 4.2). Concretely, this means averaging the model predictions over n randomly sampled rotations $\mathcal{R}_i \in \text{SO}(3)$,

$$\hat{f}'_{\theta}(x) = \int_{\text{SO}(3)} \mathcal{R}^{\top} \hat{f}_{\theta}(\mathcal{R}x) d\mu(\mathcal{R}) \approx \frac{1}{n} \sum_{i=1}^n \mathcal{R}_i^{\top} \hat{f}_{\theta}(\mathcal{R}_i x). \quad (6)$$

The limit, $\lim_{n \rightarrow \infty} E_{\text{eq}}(\mathcal{D}, f')$, converges to zero for any f'_{θ} (proof in Appendix A.4). When empirically evaluating $E_{\text{eq}}(\mathcal{D}, \hat{f}'_{\theta})$ for high values of n , we can thus attribute remaining errors to numerical inaccuracies during evaluation. We can thus grasp the numerical limit of $\text{SO}(3)$ equivariance and how close our model has approached it. In practice we approximate $\lim_{n \rightarrow \infty} E_{\text{eq}}(\mathcal{D}, f')$ by evaluating E_{eq} for multiple frame-averaging sizes n and fitting an exponential function to extrapolate to the asymptotic value for $n \rightarrow \infty$.

We evaluate MD-ET’s average E_{eq} across 2048 randomly drawn QCML train and test samples (see Figure 1, top left). The results show that without frame-averaging MD-ET reaches an E_{eq} of around 0.06 kcal/mol/Å (top left), which is one order of magnitude below our test set loss and two to three orders of magnitude below typical force magnitudes. Frame-averaging exponentially decreases the equivariance error towards a value below 0.02 kcal/mol/Å (bottom right). E_{eq} is higher on the test set, which suggests that learned equivariance might not be retained further from the training distribution. To investigate this possibility, we calculate E_{eq} for a number of alkanes (purple) and cumulenes (blue) of increasing size: Structures with more than 8 carbons are out-of-distribution (see Figure 1, top right; for visualization, see Appendix B). For each structure, we approximate the numerical noise level (see Figure 1, bottom left) using MD-ET and an equivariant SpookyNet. We also examine the ratio between the noise level and E_{eq} without frame-averaging (see Figure 1, bottom right) to evaluate how closely MD-ET approaches the practical limit for $\text{SO}(3)$ equivariance across structures.

Results demonstrate that MD-ET’s approximation of $\text{SO}(3)$ equivariance measured relative to the noise level varies little between structures, even in the extrapolative regime. On the other hand, numerical noise varies significantly between structures and tends to increase with structure size. This observation extends to the equivariant SpookyNet architecture.

For in-distribution data, we find that MD-ET learns to approximate equivariance well, approaching the limit imposed by the numerical accuracy to an order of magnitude. Given that we use only one additional data augmentation per sample during training, learning approximate equivariance appears cheap and effective. The achieved equivariance error is unlikely to impact force prediction accuracy since it is two orders of magnitude lower than typical molecular forces for most structures. Four frame-averaging samples can further reduce the equivariance error by more than 50 %. In the extrapolative regime, we observe an increase in numerical noise and larger differences in noise levels between structures. While problems with out-of-distribution generalization are widely studied, deteriorating numerical stability in the extrapolative regime is a distinct phenomenon and has a significant effect on an MLFF’s prediction quality. In contrast, learned equivariance appears to generalize well when noise levels are taken into account. We thus conclude that learning approximate equivariance is unlikely to impede a model’s accuracy, while numerical instability—which is a concern for all ML models—could.

4.5 Q3: Evaluation of Energy Conservation

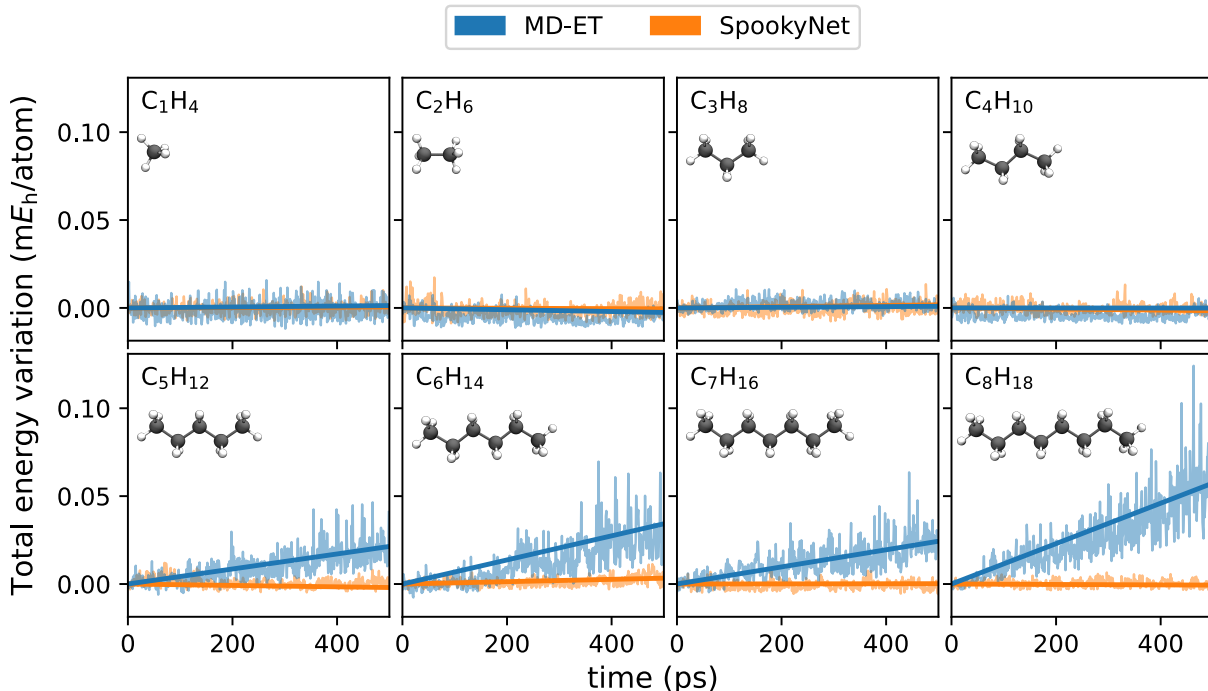


Figure 2: Total energy variation over time for NVE simulations of linear alkanes C_nH_{2n+2} ($n = 1 \dots 8$). For reference, we compare to MD simulations with an energy-conserving model (SpookyNet [13]) trained on the same data as MD-ET. A linear fit is plotted above the raw data to help visualize energy drift.

Since MD-ET directly predicts forces without enforcing energy conservation, we aim to assess whether the predicted forces are approximately conservative in addition to being approximately equivariant. Although MD-ET achieves stable MD simulations on the MD17 benchmark (see Table 2), this alone is not sufficient to demonstrate approximate energy conservation. This is because the dynamics sample the canonical (NVT) ensemble, i.e., the aim is to keep the temperature of the simulated system constant. To achieve this, a thermostat constantly introduces or removes energy, which prevents testing energy conservation. We therefore also perform MD simulations sampling the microcanonical (NVE) ensemble, where total energy is a conserved quantity. This enables quantification of how strongly a simulation violates energy conservation by monitoring the variation of total energy over time. Note that even when using conservative FFs, the total energy typically fluctuates slightly due to numerical noise and discretization errors when integrating the equations of motion. This is acceptable as long as these fluctuations are small and stay centered around zero, i.e., do not introduce energy drift. We find that NVE simulations with MD-ET are approximately energy-conserving for small systems (fewer than around 15 atoms), but for larger systems, the total energy tends to increase linearly with time (see Figure 2). The additional energy causes increasingly large structural fluctuations until the simulation invariably becomes unstable after a sufficiently large number of time steps. For many MD experiments MD-ET’s utility is thus questionable. Nevertheless, our results are surprising: To our knowledge no other approximately energy-conserving MD

model has been shown to be approximately energy-conserving and stable in short NVE simulations [29].

4.6 Q4: MD Simulation results

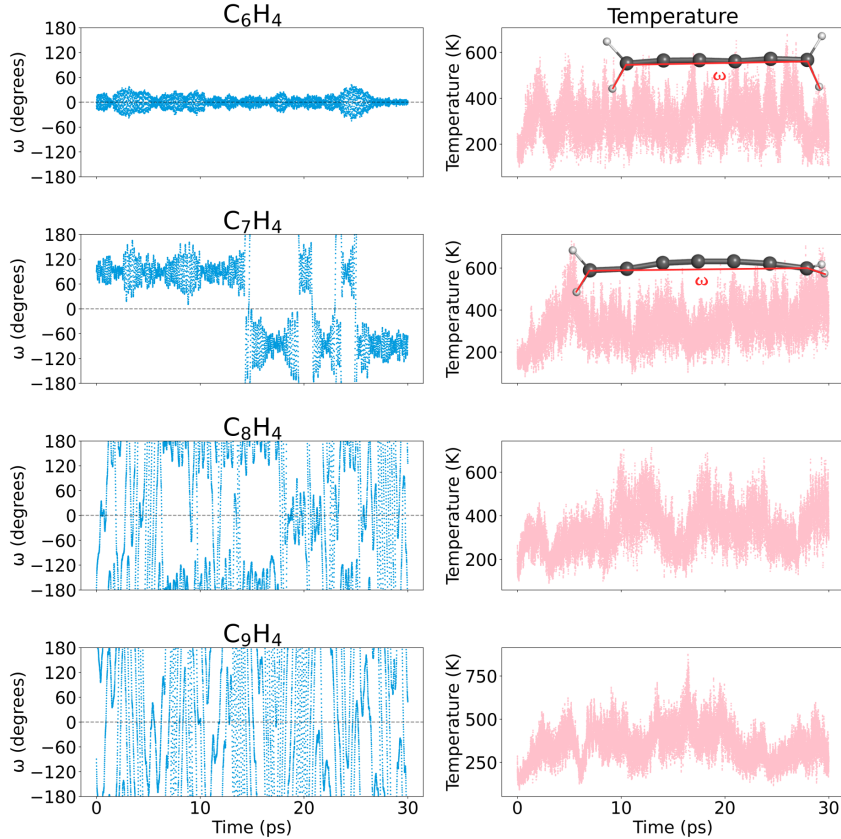


Figure 3: Left column: Dihedral angle of cumulenes of length 6 to 9 over an NVT simulation of 30 ps. Right column: Instantaneous temperature over time. The inset in the first two rows shows the flat structure of the first cumulene and the perpendicular structure in the second one. The dihedral angle ω is denoted in red, encompassing the four hydrogen atoms.

To qualitatively assess the faithfulness of an MD-ET’s simulations, we evaluate its ability to reproduce structural features in cumulenes (C_nH_4 , $n = 6-9$), where the first three are in-distribution and the last is out-of-distribution. These molecules exhibit distinct geometric patterns depending on the parity of their carbon chain length: even-numbered cumulenes adopt planar conformations with a dihedral angle $\omega \approx 0^\circ$ between the hydrogen atoms on either side, while odd-numbered chains (C_3H_4 , C_5H_4) exhibit perpendicular hydrogen arrangements ($\omega \approx 90^\circ$) due to electronic conjugation effects (see Figure 3, left). We performed NVT simulations using a Langevin thermostat ($\tau = 100$ fs) at 300 K. Each simulation spanned 60 ps with a 0.5 fs time step. Figure 3 (left) shows the time evolution of ω for all four cumulenes. For even $n = 6$, ω fluctuates around 0° , reflecting the expected planar geometry. In contrast, odd n systems exhibit ω centered near 90° , consistent with their non-planar equilibrium structures. While the model successfully captures the parity-dependent behavior for the smallest in-distribution case, it wrongly predicts relative rotation of the terminal CH₂ groups around the molecular axis (as seen by the flip of the dihedral angle). This indicates that the rotational energy barrier around the double bond is not captured correctly by MD-ET, leading to erroneous dynamical behavior.

5 Conclusion

There is an ongoing debate in the MD community whether including inductive biases such as energy conservation or rotational equivariance in ML architectures are necessary for successful MD applications. ML methods have always needed to find a balance between ease of optimization and the need to include helpful inductive biases. While traditional models for MD lean toward strong inductive biases, here, we present MD-ET, an Edge Transformer-based approach to molecular dynamics simulations that relaxes strict equivariance and energy conservation constraints during training. By predicting forces directly and utilizing data augmentation, our model achieves approximate equivariance and is approximately energy-conserving for MD simulations of small systems. MD-ET is fast, taking full advantage of the accelerators it runs on. It closely resembles a regular transformer, uses no custom layers (not counting embedding layers) and is easy to implement and use. By being “off-the-shelf”, MD-ET can profit from a vast body of research on transformers and transformer variants. It is uncomplicated to train and can quickly be applied to new datasets.

For a minimally MD-adapted architecture, MD-ET shows surprisingly good benchmark results, beating specialized architectures on several tasks measuring accuracy, speed and stability. It further displays good few-shot transfer and zero-shot capabilities, including stable zero-shot *short* MD simulations in the NVT ensemble. Longer simulations, especially in the NVE ensemble, exhibit instabilities. Such problems are also known for equivariant and energy-conserving models, where they are often associated with so-called “holes in the potential energy surface” [60].

To better understand potential problems with unconstrained architectures we experimented with MD-ET, studying potentially problematic properties. To evaluate equivariance we introduced a simple metric which is able to usefully quantify the expected error incurred by approximate equivariance and isolate it from other sources of error such as numeric instability. Results suggest that numeric instability for MD-models in general significantly varies from structure to structure and grows for larger structures and in the extrapolative regime. With regards to learning approximate energy conservation, we find that, at least with our current approach, this seems to work reasonably well for small systems of less than 15 atoms. Here too, larger systems prove more challenging.

MD-ET’s performance suggests that models for MD simulations may not necessarily need a special-purpose architecture to adhere to physical constraints, and instead, these constraints can also be learned from data. This is particularly successful for rotational equivariance, which MD-ET can learn almost up to numerical precision. Whether energy conservation can similarly be learned and whether non-conservative MLFFs can be used for reliable MD simulations of large molecular systems is questionable, at least without further advances, such as additional loss terms that encourage learning of energy-conserving forces. The disagreement of metrics commonly used by the ML community and MD simulation results is not an issue limited to MD-ET but instead raises the question how well ML benchmarks are aligned with the needs of practitioners.

Our experiments with MD-ET show an uncommon and unexpectedly successful new approach to MD (for summary see Appendix A.1). While many problems remain and unconstrained architectures such as MD-ET are still unsuitable for many MD simulations, we have promising early results. We have also identified several avenues of further investigation such as length generalization ability and the impact of numerical noise on generalization.

Software and Data

Project code is available on github: <https://github.com/mx-e/simple-md>.

Acknowledgements

We thank Luis Müller for his encouragement and being a great colleague. We also thank Elron Pens, Stefan Chmiela and Sidney Bender for important insights and fruitful discussions. Stefan Gugler was supported by the Postdoc.Mobility fellowship by the Swiss National Science Foundation (project no. 225476)

References

- [1] Daan Frenkel and Berend Smit. *Understanding Molecular Simulation: From Algorithms to Applications*. Elsevier, 2023.
- [2] Mark E. Tuckerman. *Statistical Mechanics: Theory and Molecular Simulation*. Oxford Graduate Texts. Oxford University Press, 2023.
- [3] Dominik Marx and Jürg Hutter. *Ab Initio Molecular Dynamics: Basic Theory and Advanced Methods*. Cambridge University Press, 2009.
- [4] H. Bernhard Schlegel. Geometry optimization. *WIREs Computational Molecular Science*, 1(5):790–809, 2011.
- [5] Hao Geng, Fangfang Chen, Jing Ye, and Fan Jiang. Applications of Molecular Dynamics Simulation in Structure Prediction of Peptides and Proteins. *Computational and Structural Biotechnology Journal*, 17:1162–1170, 2019.
- [6] Aparajita Chakraborty, Elisey Kobzev, Jonathan Chan, Gayan Heruka de Zoysa, Vijayalekshmi Sarojini, Thomas J. Piggot, and Jane R Allison. Molecular Dynamics Simulation of the Interaction of Two Linear Battacin Analogs with Model Gram-Positive and Gram-Negative Bacterial Cell Membranes. *ACS Omega*, 6(1):388–400, 2021.
- [7] Edward Ditler and Sandra Lubner. Vibrational spectroscopy by means of first-principles molecular dynamics simulations. *WIREs Computational Molecular Science*, 12(5):e1605, 2022.
- [8] John Jumper, Richard Evans, Alexander Pritzel, Tim Green, Michael Figurnov, Olaf Ronneberger, Kathryn Tunyasuvunakool, Russ Bates, Augustin Židek, Anna Potapenko, Alex Bridgland, Clemens Meyer, Simon A. A. Kohl, Andrew J. Ballard, Andrew Cowie, Bernardino Romera-Paredes, Stanislav Nikolov, Rishub Jain, Jonas Adler, Trevor Back, Stig Petersen, David Reiman, Ellen Clancy, Michal Zielinski, Martin Steinegger, Michalina Pacholska, Tamas Berghammer, Sebastian Bodenstein, David Silver, Oriol Vinyals, Andrew W. Senior, Koray Kavukcuoglu, Pushmeet Kohli, and Demis Hassabis. Highly accurate protein structure prediction with AlphaFold. *Nature*, 596(7873):583–589, 2021.
- [9] Oliver T. Unke, Martin Stöhr, Stefan Ganscha, Thomas Unterthiner, Hartmut Maennel, Sergii Kashubin, Daniel Ahlin, Michael Gastegger, Leonardo Medrano Sandonas, Joshua T. Berryman, Alexandre Tkatchenko, and Klaus-Robert Müller. Biomolecular dynamics with machine-learned quantum-mechanical force fields trained on diverse chemical fragments. *Science Advances*, 10(14):eadn4397, 2024.
- [10] Josh Abramson, Jonas Adler, Jack Dunger, Richard Evans, Tim Green, Alexander Pritzel, Olaf Ronneberger, Lindsay Willmore, Andrew J Ballard, Joshua Bambrick, et al. Accurate structure prediction of biomolecular interactions with alphafold 3. *Nature*, pages 1–3, 2024.
- [11] Matthias Rupp, Alexandre Tkatchenko, Klaus-Robert Müller, and O Anatole Von Lilienfeld. Fast and accurate modeling of molecular atomization energies with machine learning. *Physical review letters*, 108(5):058301, 2012.
- [12] Frank Noé, Alexandre Tkatchenko, Klaus-Robert Müller, and Cecilia Clementi. Machine learning for molecular simulation. *Annual review of physical chemistry*, 71(1):361–390, 2020.
- [13] Oliver T Unke, Stefan Chmiela, Michael Gastegger, Kristof T Schütt, Huziel E Saucedo, and Klaus-Robert Müller. Spookynet: Learning force fields with electronic degrees of freedom and nonlocal effects. *Nature communications*, 12(1):7273, 2021.
- [14] John A Keith, Valentin Vassilev-Galindo, Bingqing Cheng, Stefan Chmiela, Michael Gastegger, Klaus-Robert Müller, and Alexandre Tkatchenko. Combining machine learning and computational chemistry for predictive insights into chemical systems. *Chemical reviews*, 121(16):9816–9872, 2021.
- [15] Oliver T Unke, Stefan Chmiela, Huziel E Saucedo, Michael Gastegger, Igor Poltavsky, Kristof T Schütt, Alexandre Tkatchenko, and Klaus-Robert Müller. Machine learning force fields. *Chemical Reviews*, 121(16):10142–10186, 2021.
- [16] Stefan Chmiela, Alexandre Tkatchenko, Huziel E. Saucedo, Igor Poltavsky, Kristof T. Schütt, and Klaus-Robert Müller. Machine learning of accurate energy-conserving molecular force fields. *Science Advances*, 3(5):e1603015, 2017.

- [17] Kristof Schütt, Pieter-Jan Kindermans, Huziel Enoc Saucedo Felix, Stefan Chmiela, Alexandre Tkatchenko, and Klaus-Robert Müller. Schnet: A continuous-filter convolutional neural network for modeling quantum interactions. *Advances in neural information processing systems*, 30:992–1002, 2017.
- [18] K. T. Schütt, H. E. Saucedo, P. J. Kindermans, A. Tkatchenko, and K. R. Müller. SchNet – A deep learning architecture for molecules and materials. *The Journal of Chemical Physics*, 148(24):241722, 2018.
- [19] Nathaniel Thomas, Tess E. Smidt, Steven Kearnes, Lusann Yang, Li Li, Kai Kohlhoff, and Patrick Riley. Tensor field networks: Rotation- and translation-equivariant neural networks for 3d point clouds. *arXiv preprint*, abs/1802.08219, 2018.
- [20] Stefan Chmiela, Huziel E Saucedo, Klaus-Robert Müller, and Alexandre Tkatchenko. Towards exact molecular dynamics simulations with machine-learned force fields. *Nature communications*, 9(1):3887, 2018.
- [21] Kristof Schütt, Oliver Unke, and Michael Gastegger. Equivariant message passing for the prediction of tensorial properties and molecular spectra. In *International Conference on Machine Learning*, pages 9377–9388. PMLR, 2021.
- [22] Michael M. Bronstein, Joan Bruna, Taco Cohen, and Petar Velickovic. Geometric deep learning: Grids, groups, graphs, geodesics, and gauges. *arXiv preprint*, abs/2104.13478, 2021.
- [23] Oliver Unke, Mihail Bogojeski, Michael Gastegger, Mario Geiger, Tess Smidt, and Klaus-Robert Müller. Se (3)-equivariant prediction of molecular wavefunctions and electronic densities. *Advances in Neural Information Processing Systems*, 34:14434–14447, 2021.
- [24] Jared Kaplan, Sam McCandlish, Tom Henighan, Tom B Brown, Benjamin Chess, Rewon Child, Scott Gray, Alec Radford, Jeffrey Wu, and Dario Amodei. Scaling laws for neural language models. *arXiv preprint arXiv:2001.08361*, 2020.
- [25] Patrick Esser, Sumith Kulal, Andreas Blattmann, Rahim Entezari, Jonas Müller, Harry Saini, Yam Levi, Dominik Lorenz, Axel Sauer, Frederic Boesel, et al. Scaling rectified flow transformers for high-resolution image synthesis. In *Forty-first International Conference on Machine Learning*, 2024.
- [26] Alexey Dosovitskiy, Lucas Beyer, Alexander Kolesnikov, Dirk Weissenborn, Xiaohua Zhai, Thomas Unterthiner, Mostafa Dehghani, Matthias Minderer, Georg Heigold, Sylvain Gelly, Jakob Uszkoreit, and Neil Houlsby. An image is worth 16x16 words: Transformers for image recognition at scale. In *ICLR*, 2021.
- [27] Jan E. Gerken and Pan Kessel. Emergent equivariance in deep ensembles. In *ICML*, 2024.
- [28] Oskar Nordenfors and Axel Flinth. Ensembles provably learn equivariance through data augmentation. *arXiv preprint*, abs/2410.01452, 2024.
- [29] Filippo Bigi, Marcel F. Langer, and Michele Ceriotti. The dark side of the forces: assessing non-conservative force models for atomistic machine learning. *arXiv preprint*, abs/2412.11569, 2024.
- [30] Tycho F. A. van der Ouderaa, David W. Romero, and Mark van der Wilk. Relaxing equivariance constraints with non-stationary continuous filters. In *NeurIPS*, 2022.
- [31] Ahmed A. A. Elhag, T. Konstantin Rusch, Francesco Di Giovanni, and Michael M. Bronstein. Relaxed equivariance via multitask learning. *arXiv preprint*, abs/2410.17878, 2024.
- [32] Johann Brehmer, Sönke Behrends, Pim de Haan, and Taco Cohen. Does equivariance matter at scale? *arXiv preprint*, abs/2410.23179, 2024.
- [33] Weihua Hu, Muhammed Shuaibi, Abhishek Das, Siddharth Goyal, Anuroop Sriram, Jure Leskovec, Devi Parikh, and C. Lawrence Zitnick. Forcenet: A graph neural network for large-scale quantum calculations. *arXiv preprint*, abs/2103.01436, 2021.
- [34] Johannes Gasteiger, Florian Becker, and Stephan Günnemann. Gemnet: Universal directional graph neural networks for molecules. In *NeurIPS*, 2021.

- [35] Mark Neumann, James Gin, Benjamin Rhodes, Steven Bennett, Zhiyi Li, Hitarth Choubisa, Arthur Hussey, and Jonathan Godwin. Orb: A fast, scalable neural network potential. *arXiv preprint*, abs/2410.22570, 2024.
- [36] Yi-Lun Liao, Brandon M. Wood, Abhishek Das, and Tess E. Smidt. Equiformerv2: Improved equivariant transformer for scaling to higher-degree representations. In *ICLR*, 2024.
- [37] Leon Bergen, Timothy J. O’Donnell, and Dzmitry Bahdanau. Systematic generalization with edge transformers. In *NeurIPS*, 2021.
- [38] Luis Müller, Daniel Kusuma, Blai Bonet, and Christopher Morris. Towards principled graph transformers. In *NeurIPS*, 2024.
- [39] Stefan Ganscha, Oliver T. Unke, Daniel Ahlin, Hartmut Maennel, Sergii Kashubin, and Klaus-Robert Müller. The qcml dataset – quantum chemistry reference data from 33.5m dft and 14.7b semi-empirical calculations. (*submitted*), 2025.
- [40] John P. Perdew, Matthias Ernzerhof, and Kieron Burke. Rationale for mixing exact exchange with density functional approximations. *J. Chem. Phys.*, 105(22):9982–9985, 1996.
- [41] Carlo Adamo and Vincenzo Barone. Toward reliable density functional methods without adjustable parameters: The PBE0 model. *J. Chem. Phys.*, 110(13):6158–6170, 1999.
- [42] Eike Caldeweyher, Sebastian Ehlert, Andreas Hansen, Hagen Neugebauer, Sebastian Spicher, Christoph Bannwarth, and Stefan Grimme. A generally applicable atomic-charge dependent london dispersion correction. *The Journal of chemical physics*, 150(15), 2019.
- [43] Jan Hermann and Alexandre Tkatchenko. Density functional model for van der Waals interactions: Unifying many-body atomic approaches with nonlocal functionals. *Phys. Rev. Lett.*, 124(14):146401, 2020.
- [44] Jonathan P. Mailoa, Mordechai Kornbluth, Simon L. Batzner, Georgy Samsonidze, Stephen T. Lam, Chris Ablitt, Nicola Molinari, and Boris Kozinsky. Fast Neural Network Approach for Direct Covariant Forces Prediction in Complex Multi-Element Extended Systems. *Nature Machine Intelligence*, 1(10): 471–479, 2019.
- [45] Omri Puny, Matan Atzmon, Edward J. Smith, Ishan Misra, Aditya Grover, Heli Ben-Hamu, and Yaron Lipman. Frame averaging for invariant and equivariant network design. In *ICLR*, 2022.
- [46] Alexandre Duval, Simon V Mathis, Chaitanya K Joshi, Victor Schmidt, Santiago Miret, Fragkiskos D Malliaros, Taco Cohen, Pietro Lio, Yoshua Bengio, and Michael Bronstein. A hitchhiker’s guide to geometric gnns for 3d atomic systems. *arXiv preprint*, abs/2312.07511, 2023.
- [47] Marcel F. Langer, Sergey N. Pozdnyakov, and Michele Ceriotti. Probing the effects of broken symmetries in machine learning. *Machine Learning: Science and Technology*, 5(4):04LT01, 2024.
- [48] Christopher Morris, Yaron Lipman, Haggai Maron, Bastian Rieck, Nils M Kriege, Martin Grohe, Matthias Fey, and Karsten Borgwardt. Weisfeiler and leman go machine learning: The story so far. *The Journal of Machine Learning Research*, 24(1):15865–15923, 2023.
- [49] Snir Hordan, Tal Amir, and Nadav Dym. Weisfeiler leman for euclidean equivariant machine learning. *arXiv preprint*, abs/2402.02484, 2024.
- [50] Ashish Vaswani, Noam Shazeer, Niki Parmar, Jakob Uszkoreit, Llion Jones, Aidan N Gomez, Łukasz Kaiser, and Illia Polosukhin. Attention is All you Need. In *NeurIPS*, 2017.
- [51] Lei Jimmy Ba, Jamie Ryan Kiros, and Geoffrey E. Hinton. Layer normalization. *arXiv preprint*, abs/1607.06450, 2016.
- [52] Sheheryar Zaidi, Michael Schaarschmidt, James Martens, Hyunjik Kim, Yee Whye Teh, Alvaro Sanchez-Gonzalez, Peter W. Battaglia, Razvan Pascanu, and Jonathan Godwin. Pre-training via denoising for molecular property prediction. In *ICLR*, 2023.
- [53] Tsz Wai Ko, Jonas A. Finkler, Stefan Goedecker, and Jörg Behler. A fourth-generation high-dimensional neural network potential with accurate electrostatics including non-local charge transfer. *Nature Communications*, 12(1):398, 2021.

- [54] Linfeng Zhang, Jiequn Han, Han Wang, Wissam Saidi, Roberto Car, and Weinan E. End-to-end symmetry preserving inter-atomic potential energy model for finite and extended systems. In *NeurIPS*, 2018.
- [55] Johannes Gasteiger, Janek Groß, and Stephan Günnemann. Directional message passing for molecular graphs. In *ICLR*, 2020.
- [56] Yi Liu, Limei Wang, Meng Liu, Xuan Zhang, Bora Oztekin, and Shuiwang Ji. Spherical message passing for 3d graph networks. *arXiv preprint*, abs/2102.05013, 2021.
- [57] Simon Batzner, Albert Musaelian, Lixin Sun, Mario Geiger, Jonathan P. Mailoa, Mordechai Kornbluth, Nicola Molinari, Tess E. Smidt, and Boris Kozinsky. E(3)-equivariant graph neural networks for data-efficient and accurate interatomic potentials. *Nature Communications*, 13(1), 2022.
- [58] Xiang Fu, Zhenghao Wu, Wujie Wang, Tian Xie, Sinan Keten, Rafael Gomez-Bombarelli, and Tommi Jaakkola. Forces are not enough: Benchmark and critical evaluation for machine learning force fields with molecular simulations. *arXiv preprint*, abs/2210.07237, 2022.
- [59] Mojtaba Haghighatlari, Jie Li, Xingyi Guan, Oufan Zhang, Akshaya Das, Christopher J. Stein, Farnaz Heidar-Zadeh, Meili Liu, Martin Head-Gordon, Luke Bertels, Hongxia Hao, Itai Leven, and Teresa Head-Gordon. Newtonnet: A newtonian message passing network for deep learning of interatomic potentials and forces. *arXiv preprint*, abs/2108.02913, 2021.
- [60] Jörg Behler and Michele Parrinello. Generalized neural-network representation of high-dimensional potential-energy surfaces. *Physical review letters*, 98(14):146401, 2007.

A Appendix

A.1 Side-by-side comparison

Table 5: Comparison of different force field approaches: MD-ET, MLFF (typical learned force fields), and Traditional FF (classical potentials).

Feature	MD-ET	MLFF	Traditional FF
Equivariance (close to numerical precision)	✓	✓	✓
Energy Conservation	✗	✓	✓
Short NVE Stability	~	✓	✓
Long NVE Stability	✗	✓	✓
Short NVT Stability	✓	✓	✓
Long NVT Stability	~	✓	✓
Differentiable	✓	✓	✓
Fast (per step)	✓	✓	✓
Accurate (quantum-level)	✓	✓	✗
Low Inductive Bias	✓	~	✗

A.2 Edge Transformer Implementation

A.2.1 Molecular embedding layer details

To create initial edge representations, we combine several embeddings: i) spin & charge, ii) atomic numbers, iii) pairwise distances, and iv) pairwise directions.

Spin and charge are embedded through learned embedding layers. The total spin, $s_i \in \mathbb{N}_0$, denotes the number of unpaired electrons, and $q_i \in \mathbb{Z}$ denotes the net charge. They are jointly embedded as

$$\mathbf{z}_i = \mathbf{W}^{\text{spin}} h(s_i) + \mathbf{W}^{\text{charge}} h(q_i), \quad (7)$$

where $\mathbf{W}^{\text{spin}} \in \mathbb{R}^{D \times d_{\text{spin}}}$ and $\mathbf{W}^{\text{charge}} \in \mathbb{R}^{D \times d_{\text{charge}}}$ are learned weight matrices for spin and charge, respectively, h is a one-hot encoding and d_{spin} and d_{charge} are the sizes of the spin and charge vocabularies, respectively.

The **edge embedding** for atoms i and j is defined as

$$A_{ij} = \psi_{\text{edge}} \left(\left[\mathbf{W}^{\text{atom}} h(Z_i) + \mathbf{W}^{\text{cfg}} \tau(Z_i) + \mathbf{z}_i, \right. \right. \\ \left. \left. \mathbf{W}^{\text{atom}} h(Z_j) + \mathbf{W}^{\text{cfg}} \tau(Z_j) + \mathbf{z}_j \right] \right), \quad (8)$$

where $Z_i, Z_j \in \mathbb{N}$ are the atomic numbers and $\mathbf{W}^{\text{atom}} \in \mathbb{R}^{D \times d_{\text{atom}}}$ and $\mathbf{W}^{\text{cfg}} \in \mathbb{R}^{D \times d_{\text{cfg}}}$ are the learned weight matrices for atomic numbers and electron configuration, τ (see Appendix A.2.1), respectively. Lastly, $\psi_{\text{edge}} : \mathbb{R}^{2D} \rightarrow \mathbb{R}^D$ is an MLP that projects concatenated embeddings into the embedding space.

To embed the **pairwise distance** between atoms we use a set of $K = 128$ radial basis functions (RBF),

$$\varphi_k(x) = \frac{1}{\sqrt{2\pi}\sigma_k} \exp\left(-\frac{(x - \mu_k)^2}{2\sigma_k^2}\right) \quad (9)$$

with learnable parameters μ_k and σ_k , where the former is initialized on $\mathcal{U}(0, 7)$ and the latter on $\mathcal{U}(0, 3)$, to obtain

$$R_{ij} = \psi_{\text{dist}} \left(\sum_{k=1}^K \varphi_k(md_{ij} + b) \right), \quad (10)$$

where ψ_{dist} is an MLP and m, b , are also learnable parameters initialized as 1 and 0, respectively and d_{ij} being the interatomic distance.

Directional embeddings are created by embedding the azimuthal and polar angles ϕ and θ of the pairwise displacement vectors using $K' = 128$ Fourier kernels and a linear layer. The azimuthal frequencies

and polar frequencies are defined as

$$\omega_\phi^{k'} = \pi \left(\frac{1}{2\pi} \right)^{\frac{k'}{K'/2-1}} \quad \text{and} \quad \omega_\theta^{k'} = \pi \left(\frac{1}{\pi} \right)^{\frac{k'}{K'/2-1}}, \quad (11)$$

which covers the angular space for a sufficient K' . With the Fourier feature matrix

$$F(\phi, \theta) = [\sin(\phi\omega_\phi) \quad \cos(\phi\omega_\phi) \quad \sin(\theta\omega_\theta) \quad \cos(\theta\omega_\theta)] \quad (12)$$

the directional embedding is

$$\Gamma_{ij} = \psi_{\text{dir}}(F(\phi, \theta)), \quad (13)$$

where ψ_{dir} is another learnable linear layer.

Finally, all embeddings are added so the final edge embedding is

$$E_{ij} = A_{ij} + R_{ij} + \Gamma_{ij}. \quad (14)$$

Prediction Head & Training Objective Forces are predicted directly, i.e.,

$$\hat{\mathbf{f}}_i = \psi_3 \left(\sum_{l=1}^N \psi_l(\mathbf{x}_{il}) + \psi_2(\mathbf{x}_{lj}) \right) \in \mathbb{R}^3, \quad (15)$$

where $\psi_{\{1:3\}}$ are MLPs. The loss functional for training is

$$\mathcal{L} = \frac{1}{N} \sum_{i=1}^N \|\hat{\mathbf{f}}_i - \mathbf{f}_i^*\|_2, \quad (16)$$

where $\|\cdot, \cdot\|_2$ is the ℓ^2 norm between prediction and the ground truth, \mathbf{f}_i^* , and N is the number of atoms in the structure.

Electronic embedding The function $\tau : \mathbb{N} \rightarrow \mathbb{R}^{d_{\text{efg}}}$ maps an atomic number Z_i to a fixed electron configuration descriptor that encodes i) subshell occupancy, the number of electrons in each s , p , d , and f subshell up to the valence shell, ii) valence electrons in the outermost s (vs), p (vp), d (vd), and f (vf) subshells.

This descriptor captures an atom’s electronic structure, which governs its chemical behavior. For example, chlorine ($Z = 17$) and bromine ($Z = 35$) both have 7 valence electrons (vs = 2, vp = 5), explaining their tendency to form -1 ions. The configuration follows the Aufbau principle, with exceptions in transition metals and lanthanides/actinides accounted for empirically.

$\tau(Z_i)$ retrieves a precomputed vector from a lookup table (excerpt below). Each row corresponds to an element’s ground-state electron configuration and valence electrons. The full table spans $Z = 1$ (H) to $Z = 100$ (Fm).

Table 6: Electron configuration descriptor examples. Full table available in source code.

Z	Element	1s	2s	2p	3s	3p	...	vs/vp/vd/vf
1	H	1	0	0	0	0	...	1/0/0/0
8	O	2	2	4	0	0	...	2/4/0/0
17	Cl	2	2	6	2	5	...	2/5/0/0
35	Br	2	2	6	2	6	...	2/5/10/0
79	Au	2	2	6	2	6	...	1/0/10/14

The descriptor vector is linearly transformed by $\mathbf{W}^{\text{efg}} \in \mathbb{R}^{D \times d_{\text{efg}}}$ to produce a D -dimensional embedding. This allows the model to learn similarities between elements with analogous configurations (e.g., halogens, noble gases) directly from their electronic structure.

ET Layer implementation details

We implement MD-ET using PyTorch 2.5.1. Pseudo-code of the triangular and a comparison with regular (single-head) attention can be found in Algorithm 1 (below). To improve performance, we compile the triangular attention operation at runtime using torch compile. This necessitates rewriting triangular attention without einsums.

A.3 Inference Speed Evaluation

See Table 7 below. For runtime benchmarks, we time the forward pass of the model, including all postprocessing steps on a cloud-based V100 GPU (Throughput, Latency). Inference Time measures the pure inference time without postprocessing. To give an approximation of the performance impact of frame-averaging we report the model throughput for multiple batch sizes and structures of different sizes. To make the results more comparable to different hardware we also provide total FLOPs per forward pass.

Molecule	Batch Size	Throughput	Avg Latency (ms)	Inference Time (ms)	FLOPs
Aspirin	1	159.800	6.258	4.927	5.42×10^9
	2	157.909	6.333	5.063	1.08×10^{10}
	4	147.431	6.783	5.505	2.17×10^{10}
	8	102.680	9.739	8.458	4.33×10^{10}
	16	63.636	15.714	14.414	8.67×10^{10}
	32	35.745	27.976	26.652	1.73×10^{11}
	64	18.685	53.520	52.103	3.47×10^{11}
Ethanol	1	148.151	6.750	5.429	9.96×10^8
	2	146.148	6.842	5.586	1.99×10^9
	4	151.253	6.611	5.343	3.98×10^9
	8	153.357	6.521	5.247	7.97×10^9
	16	151.867	6.585	5.313	1.59×10^{10}
	32	115.476	8.660	7.377	3.19×10^{10}
	64	70.741	14.136	12.784	6.37×10^{10}
Naphthalene	1	150.254	6.655	5.320	3.98×10^9
	2	151.231	6.612	5.333	7.96×10^9
	4	151.409	6.605	5.332	1.59×10^{10}
	8	114.743	8.715	7.458	3.18×10^{10}
	16	70.293	14.226	12.937	6.37×10^{10}
	32	41.122	24.318	22.987	1.27×10^{11}
	64	22.033	45.387	43.976	2.55×10^{11}
Salicylic Acid	1	147.294	6.789	5.481	3.14×10^9
	2	150.733	6.634	5.371	6.29×10^9
	4	154.547	6.471	5.225	1.26×10^{10}
	8	130.698	7.651	6.407	2.52×10^{10}
	16	85.649	11.676	10.401	5.03×10^{10}
	32	51.222	19.523	18.236	1.01×10^{11}
	64	27.834	35.927	34.564	2.01×10^{11}

Table 7: Inference Speed Evaluation

A.4 Equivariance proof

See main text for the equivariance error, Eq. (5).

Proof: We first simplify the first term and substitute the equivariance property $f_\theta(\mathcal{R}\mathbf{x}) = \mathcal{R}f_\theta(\mathbf{x})$:

$$\mathbb{E}_{\mathcal{R}} [\mathcal{R}^\top f_\theta(\mathcal{R}\mathbf{x})] = \mathbb{E}_{\mathcal{R}} [\mathcal{R}^\top \mathcal{R} f_\theta(\mathbf{x})]. \quad (17)$$

Since $\mathcal{R}^\top \mathcal{R} = \mathbf{I}$ (identity matrix) for all $\mathcal{R} \in \text{SO}(3)$:

$$\mathbb{E}_{\mathcal{R}} [\mathbf{I} f_\theta(\mathbf{x})] = \mathbb{E}_{\mathcal{R}} [f_\theta(\mathbf{x})]. \quad (18)$$

The expectation $\mathbb{E}_{\mathcal{R}}[f_\theta(\mathbf{x})]$ is over \mathcal{R} , but $f_\theta(\mathbf{x})$ does not depend on \mathcal{R} . So we obtain

$$\mathbb{E}_{\mathcal{R}} [f_\theta(\mathbf{x})] = f_\theta(\mathbf{x}). \quad (19)$$

For the 2nd term we apply the equivariance property to $f_\theta(\mathcal{S}\mathbf{x})$

$$f_\theta(\mathcal{S}\mathbf{x}) = \mathcal{S}f_\theta(\mathbf{x}). \quad (20)$$

and similarly obtain

$$\mathcal{S}^\top f_\theta(\mathcal{S}\mathbf{x}) = \mathcal{S}^\top \mathcal{S}f_\theta(\mathbf{x}) = \mathbf{I}f_\theta(\mathbf{x}) = f_\theta(\mathbf{x}). \quad (21)$$

Therefore, the entire expectation over x and \mathcal{S} is

$$\mathbb{E}_{\mathbf{x}, \mathcal{S}}[\|f_\theta(\mathbf{x}) - \hat{f}_\theta(\mathbf{x})\|] = 0. \quad (22)$$

2nd Claim: $\lim_{n \rightarrow \infty} E_{\text{eq}}(\mathcal{D}, \hat{f}') = 0$ for all neural nets.

Proof: We insert $\hat{f}_\theta(x) = \frac{1}{n} \sum_{i=1}^n \mathcal{R}_i^\top \hat{f}_\theta(\mathcal{R}_i x)$ into $\mathcal{S}^\top f_\theta(\mathcal{S}\mathbf{x})$, obtaining:

$$\mathcal{S}^\top \frac{1}{n} \sum_{i=1}^n \mathcal{R}_i^\top \hat{f}_\theta(\mathcal{R}_i \mathcal{S}\mathbf{x}) \quad (23)$$

Rearranging, we obtain:

$$\frac{1}{n} \sum_{i=1}^n (\mathcal{R}_i \mathcal{S})^\top \hat{f}_\theta(\mathcal{R}_i \mathcal{S}\mathbf{x}) \quad (24)$$

We now substitute $\mathcal{R}_i \mathcal{S} = \mathcal{T}_i \in SO(3)$, obtaining

$$\frac{1}{n} \sum_{i=1}^n (\mathcal{T}_i)^\top \hat{f}_\theta(\mathcal{T}_i \mathbf{x}) \quad (25)$$

According to Kolmogorov’s law the sample mean converges to the expectation for large numbers of samples. For $\lim_{n \rightarrow \infty}$ We therefore obtain

$$\mathbb{E}_{\mathcal{T} \sim SO(3)}[\mathcal{T}^\top \hat{f}_\theta(\mathcal{T}\mathbf{x})] \quad (26)$$

Inserting into equation 5 it is trivial to see that $E_{\text{eq}}(\mathcal{D}, \hat{f}') = 0$.

A.5 Training Protocol

MD-ET was trained on the QCML dataset. We employed a cosine warmup learning rate schedule with an initial warmup phase of 5,000 steps, starting from $1e-6$ and peaking at $5e-4$. We conducted training on 8 NVIDIA A100 GPUs with 80GB memory each. Important hyperparameters include:

A.6 Experimental Setup for Benchmarks

All fine-tuning experiments employ the AdamW optimizer with $\beta_1 = 0.9$, $\beta_2 = 0.999$, and weight decay $\lambda = 1e-7$. Experiments were conducted on a single NVIDIA H100 GPU with a batch size of 500. When the full batch exceeded GPU VRAM, gradient accumulation was used. The learning rate schedule combined cosine annealing with a linear warmup: fine-tuning lasted 2000 steps if not specified differently, with the first 100 steps as warmup, and a minimum learning rate of $1e-8$. During fine-tuning, each sample was augmented with two transformations—random rotations and random reflections.

Parameter	Value
Learning Rate	5×10^{-4}
Batch Size	1024
Total Steps	880,000
Weight Decay	1×10^{-7}
Gradient Clip	1.0
Embedding Dimension	192
Number of Layers	12
Number of Heads	12
FFN Multiplier	4
3D Kernels	128
Warmup Steps	5000
EMA Decay	0.9997
Minimum Learning Rate	5×10^{-8}
Attention Dropout	0
FFN Dropout	0

Table 8: Important pretraining parameters

Table 9: Fine-tuning Hyperparameter for MD17

Molecule	Train Split Size	Val Split Size	Test Split Size	Learning Rate
Aspirin	9500	500	10000	5×10^{-5}
Ethanol	9500	500	10000	5×10^{-5}
Naphthalene	9500	500	10000	5×10^{-5}
Salicylic Acid	9500	500	10000	5×10^{-5}

A.6.1 MD17

For finetuning on the MD17 experiments we follow the experimental setup of [58], namely we sample 9500/500/10000 conformations for train/val/test splits for each molecule and evaluate the force prediction error on the test set. The hyperparameters for each molecule are shown in table 9.

For full training runs on MD17 we use the same splits as above but train the model for 250k steps and with a batch size of 250, otherwise using identical settings to pretraining on QCML (see Appendix A.5)

For the stability evaluation we run an MD simulation with a timestep of 0.5fs for 600k steps. We use a Nosé-Hoover thermostat set to 500K. To improve predictions, we use frame-averaging with $n = 4$ samples per step. For more details, see [58].

A.6.2 MD17@CCSD(T)

For the MD17@CCSD(T) experiments we adapt the experimental setup of Chmiela et al. [20] and extend the evaluation for MD-ET with a scenario with less training samples. Table 10 shows the hyperparameters for the MD17@CCSD(T) experiments.

A.6.3 Ko2020

For the dataset introduced by [53] we follow the general experimental setup of Unke et. al. [13]. We additionally randomly split a validation set from the test split to optimize the learning rate. The hyperparameters used for fine-tuning for each system are shown in table 11.

A.7 Experimental setup for evaluation of energy conservation

For the evaluation of energy conservation we run NVE simulations for 1 million using a step size of 0.5fs. To improve predictions, we use frame-averaging with $n = 16$ samples per step.

Table 10: Fine-tuning Hyperparameter for MD17@CCSD(T)

Train Split Size	Molecule	Fine-tuning Steps	Test Split Size	Learning Rate
1000 Samples	Ethanol	2000	500	5×10^{-5}
	Aspirin	2000	500	5×10^{-5}
	Benzene	2000	500	5×10^{-5}
	Malonaldehyde	2000	500	5×10^{-5}
	Toluene	2000	500	5×10^{-5}
100 Samples	Ethanol	400	500	5×10^{-5}
	Aspirin	400	500	5×10^{-5}
	Benzene	400	500	5×10^{-5}
	Malonaldehyde	400	500	5×10^{-5}
	Toluene	400	500	5×10^{-5}

Table 11: Fine-tuning Hyperparameter for Ko2020

Molecule	Train Split Size	Val Split Size	Test Split Size	Learning Rate
$C_{10}H_2/C_{10}H_3^+$	9035	50	930	5×10^{-4}
Na_8/Cl_8^+	4493	50	480	1×10^{-4}
$Ag_3^{+/-}$	9930	50	1030	5×10^{-5}
Au_2-MgO	4468	50	480	5×10^{-4}

B Visualization of molecules

Algorithm 1 Comparison between standard attention and triangular attention

```

function ATTENTION( $X : n \times d$ )
   $Q, K, V \leftarrow \text{linear}(X).\text{chunk}(3)$ 
   $\tilde{A} \leftarrow \text{einsum}(id, jd \rightarrow ij, Q, K)$ 
   $A \leftarrow \text{softmax}(\tilde{A}/\sqrt{d}, -1)$ 
   $O \leftarrow \text{einsum}(ij, jd \rightarrow id, A, V)$ 
  return  $\text{linear}(O)$ 
end function

function TRI_ATTENTION( $X : n \times n \times d$ )
   $Q, K, V^1, V^2 \leftarrow \text{linear}(X).\text{chunk}(4)$ 
   $V \leftarrow \text{einsum}(ild, ljd \rightarrow iljd, V^1, V^2)$ 
   $\tilde{A} \leftarrow \text{einsum}(ild, ljd \rightarrow ilj, Q, K)$ 
   $A \leftarrow \text{softmax}(\tilde{A}/\sqrt{d}, -1)$ 
   $O \leftarrow \text{einsum}(ij, iljd \rightarrow ijd, A, V)$ 
  return  $\text{linear}(O)$ 
end function

```

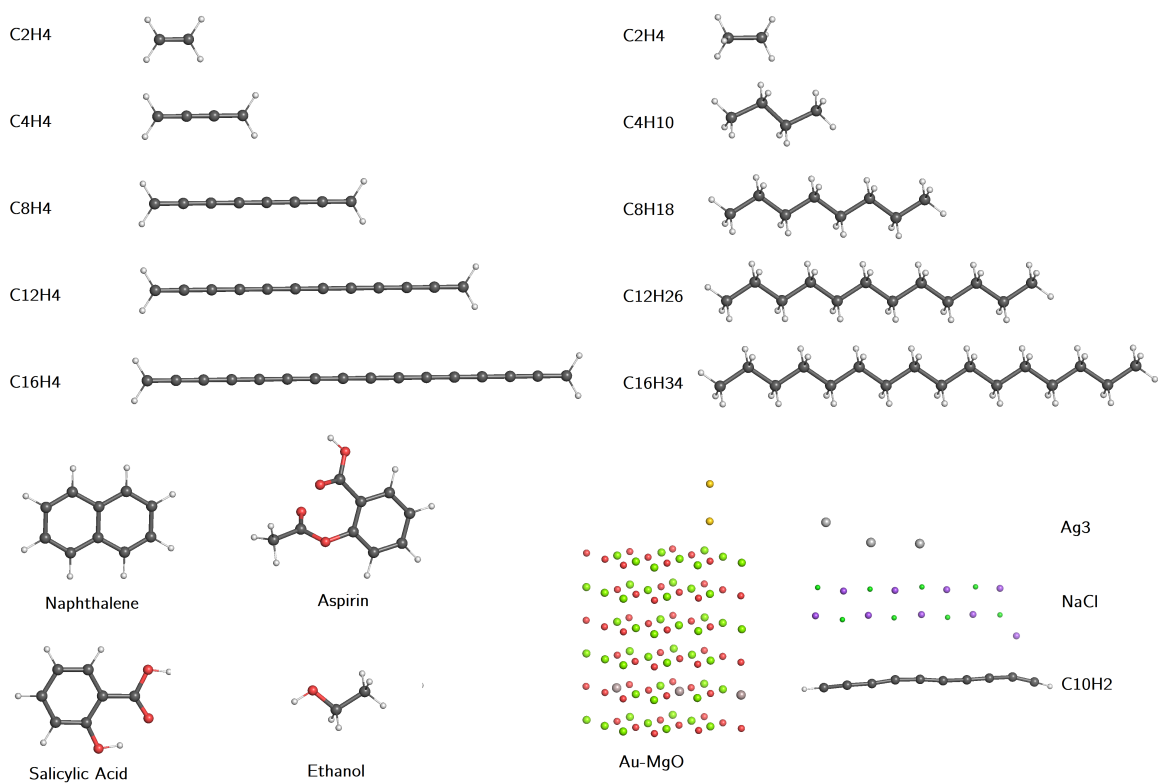


Figure 4: Visualizations of the molecular structures used in this work. In the upper half are the cumulenes (left) and the alkanes (right) with increasing carbon chain length. On the bottom left are the four molecules used from MD17: naphthalene, aspirin, salicylic acid, and ethanol. On the bottom right are the four systems studied by Ko et al. [53]: a gold dimer on a magnesium oxide surface, a silver trimer, a salt system, and C₁₀H₂ (corresponding C₁₀H⁺ omitted).